Journal of Power Sources 196 (2011) 5416–5422

Contents lists available at ScienceDirect

Journal of Power Sources

journal homepage: www.elsevier.com/locate/jpowsour

TiC supported Pt–Ir electrocatalyst prepared by a plasma process for the oxygen electrode in unitized regenerative fuel cells

Sheng Sui [a,*], Lirong Ma [b], Yuchun Zhai [b]

[a] Institute of fuel cell, Shanghai Jiao Tong University, Shanghai, China
[b] School of Materials & Metallurgy, Northeastern University, Shenyang, China

ARTICLE INFO

Article history:
Received 7 January 2011
Received in revised form 16 February 2011
Accepted 17 February 2011
Available online 26 February 2011

Keywords:
Supported electrocatalyst
Bifunctional electrocatalyst
Oxygen electrode
Chemical reduction
Plasma reduction
Unitized regenerative fuel cell

ABSTRACT

Unitized regenerative fuel cells (URFCs) have become more attractive for some time due to its potentially wide energy storage application such as in fields of space and renewable energy. In this study, TiC supported Pt–Ir electrocatalysts (Pt–Ir/TiC) for oxygen electrode in URFCs were synthesized, respectively, by chemical reduction process and plasma reduction process. Their physical and electrochemical properties are characterized and compared using X-ray diffraction (XRD), X-ray photoelectron spectroscopy (XPS), transmission electron microscopy (TEM), cyclic voltammogram (CV), potentiostatic technique, and electrochemical impedance spectroscopy (EIS). The results from XRD, XPS and TEM demonstrate that the plasma process gives a finer metal crystals and higher metal dispersion on the TiC support. The CV, polarization, potentiostatic and EIS results show that the Pt–Ir/TiC electrocatalyst prepared by the plasma reduction process is obviously more active than that by the chemical reduction process, in agreement with the above metal-dispersion observations. The plasma process is a promising way for the preparation of supported electrocatalysts.

1. Introduction

Hydrogen as an energy storage medium, which stores electrical energy by splitting water into hydrogen and oxygen, is preferably connected to a renewable energy source, such as solar or wind energy. Unitized regenerative fuel cells (URFCs), using hydrogen as the medium, is a compact energy storage unit where the water electrolyser (WE) and the fuel cell (FC) are combined into one unit and only one of the two modes can be operated at one time [1]. In the WE mode, hydrogen and oxygen are generated by splitting water using electrical power. In the FC mode, the hydrogen and oxygen or air are combined to generate water and give off electricity. Compared with conventional secondary batteries (for example, lead acid and Li-ion batteries) as storage systems, URFCs have many advantages in long-term energy storage, including high energy density, high durability and low environmental impact. They can be applied in many different areas, such as high-altitude long-endurance airship, hybrid energy-storage/propulsion systems for spacecraft, energy storage for remote (off-grid) power sources, and peak shaving for on-grid applications [2].

One of the most difficult challenges in the development of the URFCs is to improve the performance of their oxygen electrodes, and more specifically, to improve the performance of the bifunctional electrocatalysts for the oxygen electrodes [3].

To date, typical bifunctional electrocatalysts for oxygen redox reaction of URFC include Pt–Ir, Pt–Ru–Ir, Pt–IrO_2 and Pt–IrO_2–RuO_2. Most of the above described bifunctional oxygen electrode electrocatalysts are obtained by mixing an efficient electrocatalyst for oxygen reduction – Pt black, and an efficient electrocatalyst for oxygen evolution – Ir or IrO_2 or IrO_2–RuO_2, which may result in a slightly decreased performance in either the oxidation or the reduction reaction (depending on catalyst composition) and thus a lower bifunctional performance of the oxygen-electrode electrocatalysts. The electrocatalyst compositions need to be optimized for a given system application. Yim et al. [3] optimized Pt–Ir electrocatalyst for URFC and concluded that Pt–Ir catalyst with 1 wt.% Ir revealed the highest URFC efficiency. Grigoriev et al. [4] recently suggested anodic bifunctional electrocatalytic structures for URFCs based on proton exchange membrane (PEM) technology. Among various Pt–Ir compositions, the best URFC performances were reported to be obtained with two adjacent porous layers, of which the first layer was made of Ir (50 wt.%) in direct contact with the polymer membrane and the second layer was made of Pt (50 wt.%) and coated over the first one.

Several factors influence the electrocatalytic activity of the catalysts for the oxygen evolution reaction, including the crystal-field stabilization energy, mixed and doped oxides, catalyst dispersion, crystallinity, and crystallite size [5]. IrO_2/Pt can be prepared by

* Corresponding author. Tel.: +86 21 34206249; fax: +86 21 34206249.
E-mail address: ssui@sjtu.edu.cn (S. Sui).

0378-7753/$ – see front matter © 2011 Elsevier B.V. All rights reserved.
doi:10.1016/j.jpowsour.2011.02.058

deposition of the colloid precursor $Ir(OH)_3(H_2O)_3$ on Pt black. Ioroi et al. [6] reported that the catalytic performance of the deposited IrO_2/Pt is better than that of mixed IrO_2/Pt because it is relatively easy to maintain the conduction path of electrons along Pt agglomerates in the deposited IrO_2/Pt catalyst, while the electron conduction path tends to be hindered by IrO_2 agglomerates in the mixed IrO_2/Pt catalysts.

On the contrast, Yao et al. [7] reported that platinum nanoparticles deposited on the surface of IrO_2 by chemical reduction, compared to the mixture or Pt and IrO_2, showed distinct behaviors in the oxygen reduction reaction (ORR) and in the oxygen evolution reaction (OER). As a bifunctional electrocatalyst for oxygen electrode, IrO_2-supported Pt exhibits slightly lower ORR activity but markedly higher OER activity than the mixture of Pt and IrO_2. They explained it by the downshift of the d-band center energy through the d-band coupling, therefore resulting in a weaker O_2 molecule adsorption on Pt catalysts supported by IrO_2. Zhang et al. [8] synthesize a bifunctional RuO_2–IrO_2/Pt electrocatalyst for the URFC by colloid deposition. URFC with the deposited RuO_2–IrO_2/Pt showed better performance than that of URFC with mixed RuO_2–IrO_2/Pt catalyst. Cyclic performance of URFC with deposited RuO_2–IrO_2/Pt was reported very stable during 10 cyclic tests.

To reduce the loading of the noble metals, supports are used in the bifunctional electrocatalysts. Chen et al. [9] examined three oxide supports: Ebonex (primarily composed of Ti_4O_7), phasepure microcrystalline Ti_4O_7 and $Ti_{0.9}Nb_{0.1}O_2$, a doped rutile compound. These supports improve activity, but have short-lived electrochemical stability. We [10] reported recently that the catalytic activity of the Ir/TiC for the OER is significantly higher than that of the unsupported Ir catalyst. The TiC support is chemically and electrochemically stable in the whole range of experimental potentials.

Many conventional methods are used in the electrocatalyst preparation, such as chemical reduction by HCHO, KBH_4 or $NaBH_4$, the electrochemical deposition and chemical vapor deposition (CVD) [11–14].

Recently, plasma reduction has attracted more attention. Plasma can enhance or assist deposition of catalytically active compounds on various supports and produce ultrafine catalyst particles [15]. Legrand et al. [16] used the afterglow of a hydrogen microwave plasma for the preparation of zeolite yttrium (Y) supported gold and platinum nanoparticles. Kim et al. [17] reported that a hydrogen atmospheric dielectric-barrier plasma could be used as the reducing agent to prepare supported Pt and Co catalysts. Liu et al. [18–23] had used argon glow discharge plasma at room temperature to prepare Pd, Pt, Pt/Al_2O_3 and Rh/Al_2O_3 catalysts and noticed these catalysts were reduced during the process of plasma treatment.

In the present study, we prepared two kinds of Pt–Ir/TiC electrocatalysts, respectively, by chemical reduction and plasma reduction processes, and characterized them by physical and electrochemical measurements.

2. Experimental equipment and procedures

2.1. Preparation of the Pt–Ir/TiC electrocatalyst by thermal reduction process

The Pt–Ir/TiC electrocatalyst prepared by thermal reduction was made by chemical reduction and deposition with ultrasonic dispersion described in our early investigation [10]. TiC powder is a commercial product purchased from Fujian Sinocera Advanced Materials Co., Ltd. Its main physical and chemical characteristics are described as follows: TiC purity >99%, cubic structure, surface area 14.41 $m^2\,g^{-1}$, and particle size 100–200 nm. Briefly, the support TiC powders were wetted in de-ionized water containing an appropriate amount of isopropanol to form a suspended phase. The slurry was dispersed in an ultrasonic reactor for 10 min at room temperature. $H_2PtCl_6{\cdot}6H_2O$ (analytical grade) and $(NH_4)_2IrCl_6$ (Alfa Aesar) were added to the above slurry in the calculated amount for the desired loading. The aqueous solution was subsequently heated to 80 °C and stirred under ultrasonic agitation. The reducing agent (HCHO:NH_3:$H_2O \approx 2{:}1{:}21$, weight ratio) was added to the mixture at 80 °C over a period of 40 min and the mixture was kept at 80 °C under ultrasonic agitation for an hour. After cooling to room temperature, the reduced and precipitated slurry was washed repeatedly with de-ionized water until the content of chlorine anion (Cl^-) in the filtrate was less than 40 ppm. After drying at 80 °C for an hour, the filter cake was then set in a tube furnace and annealed at 500 °C for 30 min under flowing argon before cooling down to room temperature. The Pt–Ir electrocatalyst loading on the TiC support was 40 wt.%. The sample is labeled as S1.

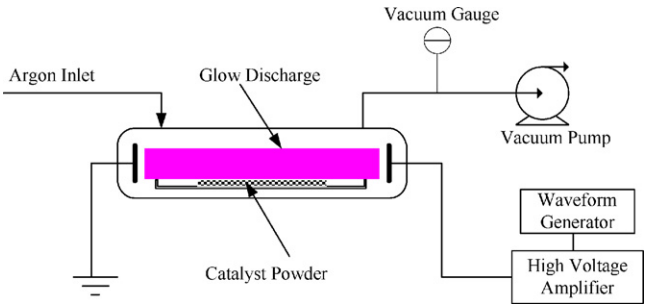

Fig. 1. Schematic setup of glow discharge plasma catalyst reduction.

2.2. Preparation of the Pt–Ir/TiC electrocatalyst by plasma reduction

The novel Pt–Ir/TiC electrocatalyst was prepared by plasma reduction. The TiC powders were first wetted in de-ionized water containing an appropriate amount of isopropanol to form a suspended phase. The slurry was dispersed in an ultrasonic reactor for 10 min at room temperature. $H_2PtCl_6{\cdot}6H_2O$ (analytical grade) and $(NH_4)_2IrCl_6$ (Alfa Aesar) were added to the above slurry in the calculated amount for the desired loading. This aqueous solution was subsequently heated to 80 °C and stirred under ultrasonic agitation for 3 h. After drying at 80 °C for 15 h, the cake was mashed and followed by plasma reduction. The plasma reduction was conducted using argon glow discharge. Details of the plasma setup were given elsewhere [20–23]. The sample (about 0.4 g), loaded on a quartz boat, was placed in the glow discharge chamber which was a horizontal quartz tube (i.d. 35 mm) with two stainless steel electrodes (o.d. 30 mm). The system was connected to a source of Ar and was evacuated with a vacuum pump. When the argon pressure was adjusted to 50–100 Pa, the glow discharge plasma was generated by applying 900 V to the electrodes using a high voltage amplifier (Trek, 20/20B), with high purity argon (>99.999%) as the plasma-forming gas. The current was in the range of 1–2 mA. The signal input for the high voltage amplifier was supplied by a function/arbitrary waveform generator (Hewlett-Packard, 33120A) with a 100 Hz square wave. The plasma reduction lasted for 10 min at each time. Because the plasma reduction is a surface reaction, the sample was stirred using a glass rod after the plasma reduction and reduced several times. Here each sample was reduced 6 times. The gas temperature of plasma was measured by infrared imaging (Ircon, 100PHT), indicating that the reduction was conducted at ambient temperature. The schematic setup of plasma reduction is shown in Fig. 1. The loading of the Pt–Ir electrocatalyst supported on the TiC is the same with the S1, but is labeled as S2.

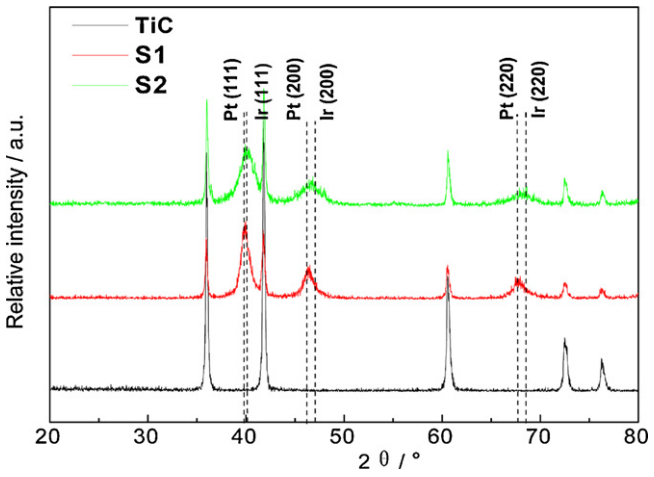

Fig. 2. XRD patterns for TiC, S1 and S2 electrocatalysts.

2.3. Physical characterization

The X-ray diffraction (XRD) pattern was recorded using a Rigaku D/max2000 with an area detector using a Cu Kα radiation source (λ = 1.54056 Å) operating at 40 kV and 20 mA. The XRD samples were obtained by placing the test samples on a glass slide and then drying under vacuum overnight. The scanning angle (2θ) region between 20° and 80° was explored at a scan rate of 0.02° s^{-1}. The particle size and surface of the electrocatalysts were determined by transmission electron microscopy (TEM) using a JEOL JEM-2010 microscope operated at 200 keV. The TEM samples were prepared by placing a drop of catalyst suspension in ethanol on a 3-mm size copper grid, followed by drying at ambient conditions. X-ray photoelectron spectra (XPS) analysis was performed using a Kratos AXIS $Ultra^{DLD}$ system operated under Al Ka radiation (1486.6 eV) with a monochromator. Binding energies calibrated with respect to C (1s) at 284.6 eV were accurate within ±0.2 eV. For XPS analysis, the powder samples were placed in an ultra high vacuum chamber at 10^{-9} Torr housing the analyzer. Before put in the analyzing chamber, the sample was kept in the preparation chamber at 10^{-9} Torr for overnight to expel any volatile species.

2.4. Working electrode preparation

Appropriate amounts of electrocatalysts were ultrasonically suspended in a small quantity of a mixture of de-ionized water, isopropanol and the calculated mass of Nafion solution (5 wt.% Nafion, Dupont) to prepare the electrocatalysts ink. Then, 5 μl of ink was taken with a transfer pipette and deposited on a clean glassy carbon electrode with an area of 0.07069 cm^2 (CHI 104, CH Instrument Co.) held in a Teflon cylinder. The electrode was dried under an infrared lamp at 40 °C for 10 min. A uniform electrocatalyst layer was obtained as the working electrode. The loading of the Pt–Ir/TiC electrocatalysts on the working electrode was about 0.02 mg.

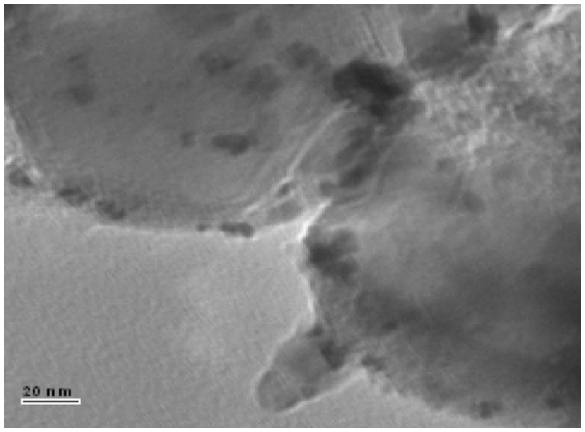

Fig. 3. TEM image for the S1 electrocatalysts.

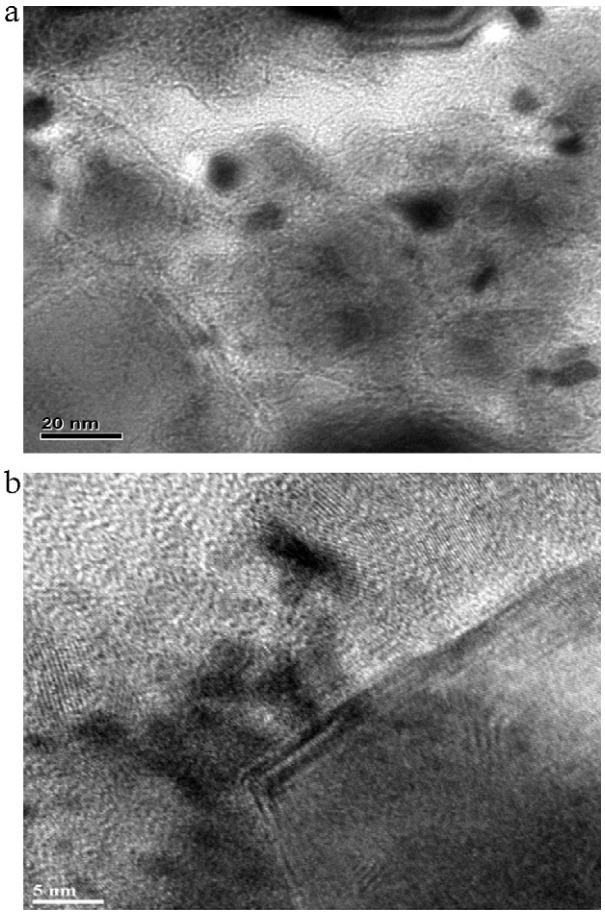

Fig. 4. TEM and HRTEM images for S2 electrocatalysts.

2.5. Electrochemical characterization

In order to determine the electrocatalytic activity of the Pt–Ir/TiC electrocatalysts (S1 and S2) for the oxygen electrode, cyclic voltammograms (CV), polarization, potentiostatic measurement and electrochemical impedance spectroscopy (EIS) characterizations were carried out at room temperature (23 ± 2 °C). The electrochemical experiments were done in a glass electrochemical cell with a three-electrode configuration. A saturated calomel electrode (SCE) in saturated potassium chloride (KCl) solution, which was positioned as close as possible to the working electrode by means of a Luggin capillary, was used as the reference electrode. The counter electrode was a 1 cm × 1 cm platinized Pt foil. The working electrode was made as described in Section 2.4 with S1 or S2 electrocatalyst. All potentials reported in this work were with respect to the SCE.

All the experiments were performed in 0.5 M H_2SO_4 solution prepared with high-purity sulfuric acid and deionized water. The potential range of the CV measurement was between −0.241 and +1.0 V with a scan rate of 50 mV s^{-1}. The electrolyte solution and surfaces of the electrodes were de-aerated with nitrogen bubbling before and during the experiments. The polarization measurements

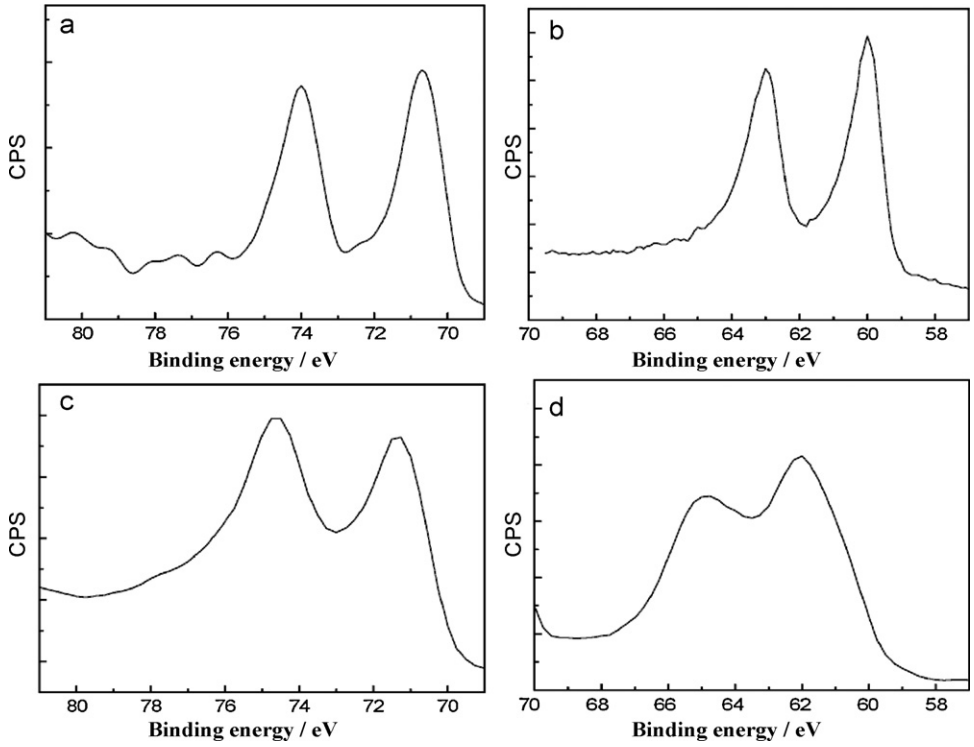

Fig. 5. XPS images for the S1 and S2 electrocatalysts. (a) Pt (4f) for the S1; (b) Ir (4f) for the S1; (c) Pt (4f) for the S2; and (d) Ir (4f) for the S2.

were recorded at the potential range of 0.6–1.5 V in the electrolyte saturated with nitrogen for the oxygen evolution reaction (OER), and 0.8–0.2 V in the electrolyte saturated with oxygen for the oxygen reduction reaction (ORR), respectively. The potentiostatic tests were carried out at the potentials of 1.3 V and 0.6 V for 600 s for the OER and the ORR, respectively, with the electrolytes being saturated with the corresponding gases as described above. All the data were collected using a Solartron Electrochemical Interface (model SI 1287) and the Corrware software. EIS experiments were carried out at frequencies from 100 kHz to 0.1 Hz. The impedance spectra were registered with a logarithmic data collection scheme at 10 steps per decade with amplitude of 10 mV at the potential of 1.2 V and 0.6 V with corresponding gases saturated. The impedance characterization was completed using a Solartron Impedance/Gain-Phase Analyzer (model SI 1260) combined with a Solartron Electrochemical Interface (model SI 1287) and the Z-plot and Z-view software were used for data processing.

3. Results and discussion

3.1. Physical characterization and analysis

The phase compositions and crystal structures of the S1 and S2 electrocatalysts were determined by XRD analysis using the TiC as an internal standard. The XRD patterns are given in Fig. 2. The characteristic intense diffraction peaks of Pt (1 1 1), Ir (1 1 1), Pt (2 0 0), Ir (2 0 0), Pt (2 2 0) and Ir (2 2 0) can be found for the S1 and S2 electrocatalysts. The labeled lines and reflection planes represent that of pure Pt and Ir metals. The characteristic peaks on the 2θ values of 39.8°, 46.2° and 67.4°, could be assigned to the reflection planes (1 1 1), (2 0 0) and (2 2 0) of a Pt. The diffraction peaks on 40.7°, 47.3° and 69.2° are due to Ir (1 1 1), (2 0 0) and (2 2 0) plane, respectively. It is expected some alloying of Pt and Ir and be from two/multiple phases that are either Ir rich or Pt rich from overlapping peaks of the XRD patterns, even although we were not able to confirm the existence of Ir rich or Pt rich phases in the microscope. At the same time, the obvious broadening of the corresponding diffraction peaks can be seen for the S2 compared with that for the S1. It demonstrates that the crystallite sizes of Pt and Ir dispersed on the TiC support in the S2 are smaller than those in the S1, respectively. The active components with smaller particle sizes and crystallites will produce more crystal lattice defects and have more highly active sites. Obviously, a high density of surface active sites and some alloying of Pt and Ir will benefit and improve the electrocatalytic activity.

The particle size and size distribution for the S1 and S2 electrocatalysts were investigated by TEM and shown in Figs. 3 and 4, respectively. They all show that the Pt and Ir nanoparticles are uniformly and highly dispersed over the TiC surface. For the S1 as represented in Fig. 3, the sizes of the particle deposited on the TiC are not well defined, with the particle size distribution in a wide range of 10–40 nm, possibly due to a certain agglomeration of the particles or sintering during sample preparation. As shown in Fig. 4, the particle size distribution of the S2 is narrower and the average diameter is about 2–5 nm, which is remarkably smaller in comparison with that of the S1. This result is accordant with the analysis of the XRD.

In order to investigate the valence states of elements on the electrocatalyst surface by binding energy, XPS tests were made and shown in Fig. 5. Fig. 5(a) and (b) are for the S1. Table 1 gives binding energies of X-ray photoelectron spectra for Pt and Ir metals. Fig. 5(c) and (d) are for the S2. It can be seen from the Pt (4f) peaks for the S1 and S2 electrocatalysts represented in Fig. 5(a) and (c), the distances between two characteristic peaks of each sample are all about 3.3 eV. The peaks in Fig. 5(a) are formed near 70.9 and

Table 1
Binding energies of X-ray photoelectron spectra for Pt and Ir metals.

Element	Binding energy (eV)	
	$4f_{5/2}$	$4f_{7/2}$
Pt	74.25	70.9
Ir	63.55	60.6

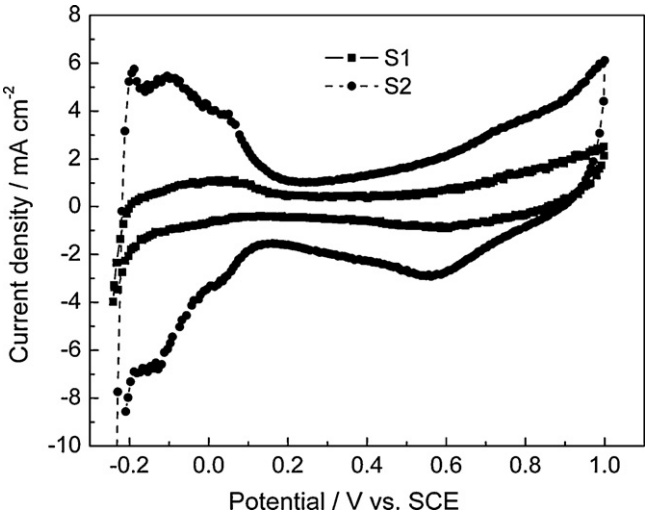

Fig. 6. CV curves for the S1 and S2 electrocatalysts.

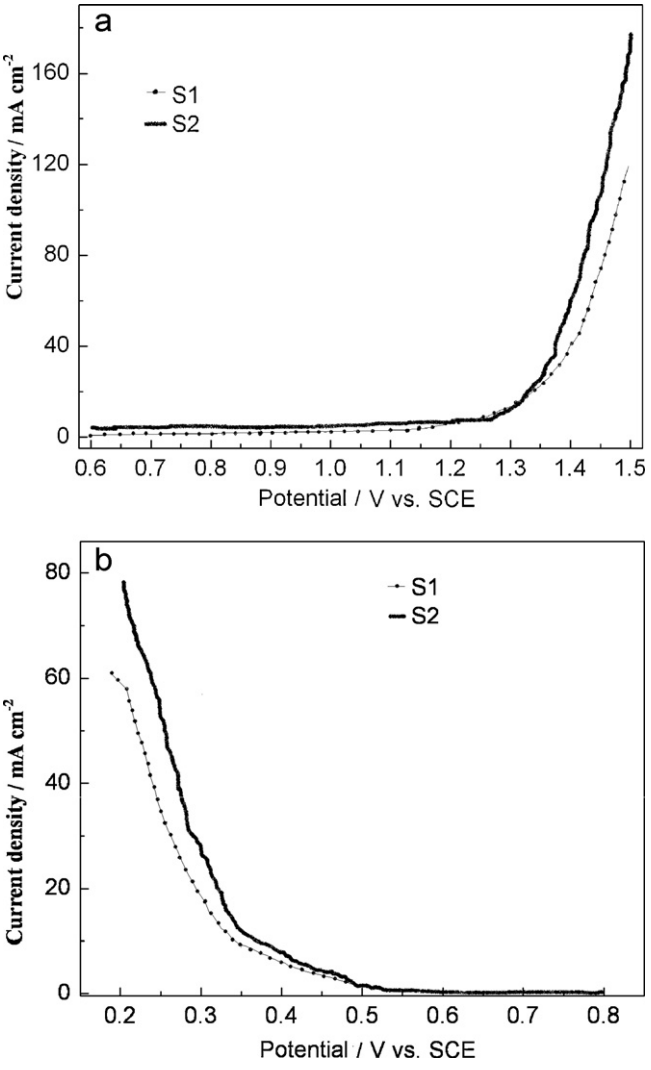

Fig. 7. Polarization curves for the S1 and S2: (a) at 0.6–1.5 V and (b) at 0.8–0.2 V.

74.2 eV, and in Fig. 5(c), near 71.3 eV and 74.6 eV which correspond to the ($4f_{7/2}$) and ($4f_{5/2}$), respectively. In Liu et al.'s work [22], they attribute the peaks at 76.3 and 72.9 eV to ($4f_{7/2}$) and ($4f_{5/2}$) transitions of platinum ion, and those at 74.1 and 71.1 eV to the energy levels of platinum metal.

As for the Ir (4f) peaks, the distances between two characteristic peaks for each sample are all about 3.0 eV as shown in Fig. 5(b) and (d). At the same time, it can be seen the Pt (4f) and Ir (4f) peaks for the S2 electrocatalyst shift to higher binding energy as compared to those peaks of the S1. Those peaks formed at about 71.3 and 74.6 eV in Fig. 5(c) are, respectively, corresponding to the ($4f_{7/2}$) and ($4f_{5/2}$) of Pt^{3+} or Pt^{4+}. Similarly, the peaks appeared about at 62.0 and 64.9 eV in Fig. 5(d) are, respectively, for Ir^{4+} ($4f_{7/2}$) and Ir^{4+} ($4f_{5/2}$). However, the Pt (4f) peaks observed at about 70.9 and 74.2 eV in Fig. 5(a) are ascribed to Pt^0 ($4f_{7/2}$) and Pt^0 ($4f_{5/2}$). And the Ir (4f) peaks appearing at about 60.0 and 63.0 eV in Fig. 5(b) correspond to Ir^0 ($4f_{7/2}$) and Ir^0 ($4f_{5/2}$). So, the XPS results indicate that the plasma treatment induces change of the electronic valence states of the Pt and Ir particles. However, we find no characteristic peaks for Pt oxide or Ir oxide in the XRD pattern of the S2. This conflict results may be due to the intense effect of electronic structure induced by the plasma treatment.

3.2. Electrochemical performance and analysis

CV investigations shown in Fig. 6 were carried out to evaluate the electrocatalytic activities of the S1 and S2. The peaks appearing at the potential of about −0.12 V provide the information on the hydrogen adsorption and desorption. Between 0.0 V and 0.2 V is the region of electric double layer. Starting from a positive potential of about 0.6 V, the S2 electrode shows a trend of relatively quick oxygen evolution compared with that of the S1. Moreover, oxygen reduction peak beginning from about 0.8 V at reverse scan is more obvious on the S2 electrode than that on the S1. It is common to take the peak current density kinetically controlled for comparison. At a positive potential of 1.0 V, the corresponding current densities are 2.5 mA cm^{-2} on the S1 electrode and 6.1 mA cm^{-2} on the S2 electrode. At 0.6 V at reverse scan, it is about 0.9 mA cm^{-2} on the S1 electrode and 2.7 mA cm^{-2} on the S2 electrode. All of these results obviously indicate that the S2 prepared by the plasma reduction treatment results in comparatively higher current densities of the dynamical process for both the oxygen evolution and the reduction, and thus its electrocatalytic activity is higher than that of the S1 at the same experimental potential.

Based on results of Fig. 6, polarization curves of the two samples were measured, respectively, at the potential range of 0.6–1.5 V saturated with nitrogen for the oxygen evolution reaction (OER), and at 0.8–0.2 V saturated with oxygen for the oxygen reduction reaction (ORR) shown in Fig. 7. In Fig. 7(a), it can be easy found that the OER current densities on the S2 electrode reveal larger values and increase more quickly than that on the S1 electrode at the same range of potentials. In addition, the S2 electrode exhibits higher current density for the ORR than that the S1 electrode at the same experiment potentials as shown in Fig. 7(b). This proves that the S2 prepared by plasma reduction has higher electrocatalytic activities for both the OER and the ORR.

Potentiostatic analysis is also used to check the performance of the S1 and S2 as the OER and ORR electrocatalysts. When evaluating the electrocatalytic activities of the S1 and S2, the potential is selected at 1.3 V and 0.6 V, respectively, according to Fig. 7(a) and (b), and the solution is saturated with N_2 and O_2, respectively. The electrolyte solution was purged with corresponding gases for 120 s before data collection. The electric charge–time curves for the OER of the S1 and S2 electrocatalysts were recorded while the working

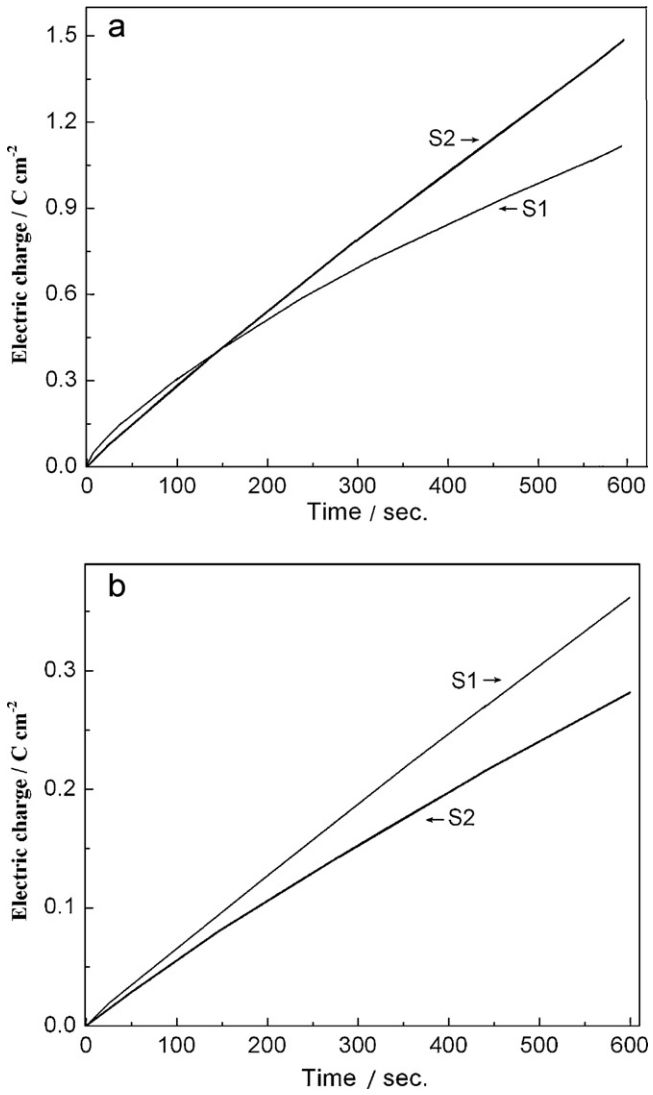

Fig. 8. Electric charge–time curves of the S1 and S2: (a)at 1.3 V and (b) at 0.6 V.

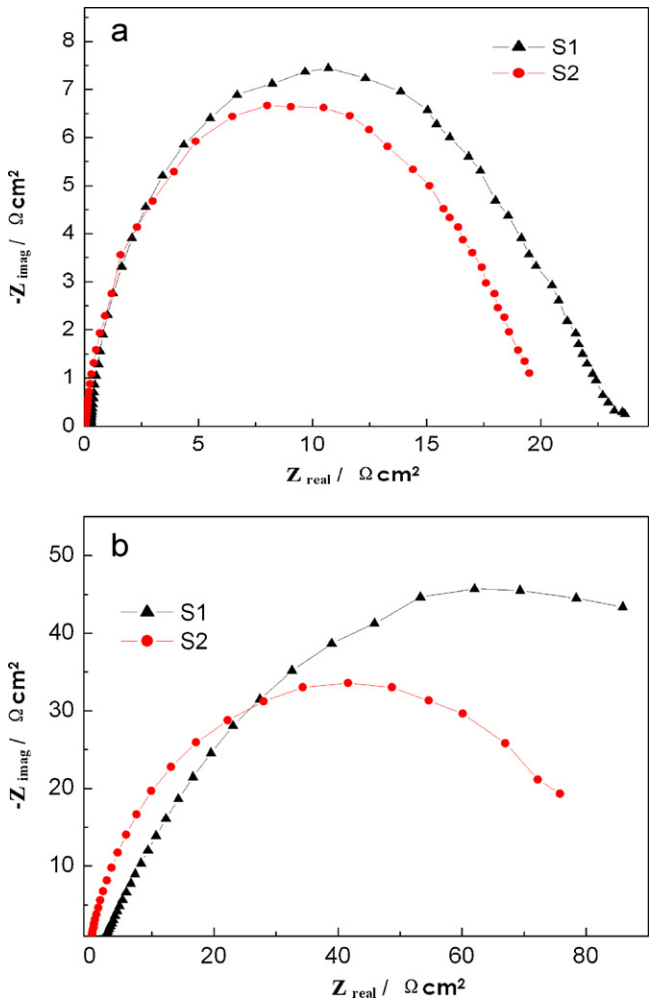

Fig. 9. EIS curves for the S1 and S2 electrodes: (a) at 1.2 V and (b) at 0.6 V.

electrodes were held at 1.3 V for 600 s, and those for the ORR were investigated at 0.6 V for 600 s, as shown in Fig. 8(a) and (b). The columbic charge passed through the two electrodes are, respectively, about 1.1 C cm^{-2} for the S1 and 1.2 C cm^{-2} for the S2 after 600 s at 1.3 V as shown in Fig. 8(a). At the same time, the columbic charges are 0.21 C cm^{-2} for the S1 and 0.28 C cm^{-2} for the S2 after 600 s at 0.6 V. So, at the applied potentials, the S2 electrode exhibits a higher passage of electric charge in both tests and shows a higher electrocatalytic activity for both OER and ORR, compared with the S1 electrode.

EIS technique has been used to investigate the kinetics and mechanisms of the electrode reactions. Nyquist plots of S1 and S2 at the electrode potential of 1.20 V and 0.6 V are recorded and shown in Fig. 9. At the comparatively high potential of 1.2 V, the reaction rate is controlled mainly by diffusion. In the range of middle and low frequency, diffusion polarization impedances of S2 are obviously lower than those of S1. These results confirm that the S2 electrode presents much lower charge transfer and diffusion resistances compared to the S1 electrode. Then the S2 electrode with lower impedances reveals correspondingly high electrocatalytic activity. All these are consistent with the results of the CV, polarization and potentiostatic measurements.

4. Conclusion

The two kinds of Pt–Ir/TiC electrocatalysts were prepared, respectively, by chemical reduction and deposition process and by plasma reduction process. The plasma treatment induces some change in the electronic states of the Pt and Ir particles. Compared with the Pt–Ir/TiC electrocatalyst prepared by chemical reduction and deposition, the novel Pt–Ir/TiC electrocatalyst prepared by plasma reduction displays the finer particles (<5 nm) and relatively uniform distribution on the support TiC surface and significant improvement in the electrocatalytic activity both for the OER and for the ORR deduced from the results of the CV, polarization, potentiostatic and EIS measurements. It also confirms that the plasma processes is a promising way for the preparation of supported electrocatalysts.

Acknowledgements

This work was financially supported by the National High Technology Research and Development Program ("863" Program) of China (Grant No. 2009AA05Z116), Science and Technology Committee of Shanghai Municipality (Grant No. 09510701400), and the National Natural Science Foundation of China (Grant No. 20576071). We also thank Professor Changjun Liu at Tianjing University for plasma treatment and the Instrumental Analysis Center at Shanghai Jiao Tong University for their help on TEM tests.

References

[1] A. Brassard, Regenerative fuel cell system, US Patent 6,579,638 (2003).
[2] Fred Mitlitsky, Blake Myers, Andrew H. Weisberg, Energy & Fuels 12 (1998) 56–71.
[3] Sung-Dae Yim, Gu-Gon Park, Young-Jun Sohn, Won-Yong Lee, Young-Gi Yoon, Tae-Hyun Yang, Sukkee Um, Sang-Phil Yu, Chang-Soo Kim, International Journal of Hydrogen Energy 30 (2005) 1345–1350.
[4] S.A. Grigoriev, P. Millet, K.A. Dzhus, H. Middleton, T.O. Saetre, V.N. Fateev, International Journal of Hydrogen Energy 35 (2010) 5070–5076.
[5] S.L. Morales, L.G. Arriaga, U. Cano, R. Acosta, ECS Transactions, vol. 3. Proton Exchange Membrane Fuel Cells 6, The Electrochemical Society, NJ, USA, 2006, p. 115.
[6] T. Ioroi, N. Kitazawa, K. Yasuda, Y. Yamamoto, H. Takenaka, Journal of Applied Electrochemistry 31 (2001) 1179–1183.
[7] Wenli Yao, Jun Yang, Jiulin Wang, Yanna Nuli, Electrochemistry Communications 9 (2007) 1029–1034.
[8] Yangjian Zhang, Cheng Wang, Nianfang Wan, Zongqiang Mao, International Journal of Hydrogen Energy 32 (2007) 400–404.
[9] Guoying Chen, Chad C. Waraksa, Hungoo Cho, Digby D. Macdonald, Thomas E. Mallouk, Journal of the Electrochemical Society 150 (9) (2003) E423–E428.
[10] Lirong Ma, Sheng Sui, Yuchun Zhai, Journal of Power Sources 177 (2008) 470–477.
[11] Ying-ying Dai, Qiang Gong, Zhen-tai Liu, Zi-feng Ma, Chemical Industry and Engineering Progress 23 (7) (2004) 731–735.
[12] Guoying Chen, David A. Delafuente, S. Sarangapani, Thomas E. Mallouk, Catalysis Today 67 (2001) 341–355.
[13] A. Marshall, B. Børresen, G. Hagen, M. Tsypkin, R. Tunold, Electrochimica Acta 51 (2006) 3161–3167.
[14] A.L. Ocampo, M. Miranda-Hernández, J. Morgado, J.A. Montoya, P.J. Sebastian, Journal of Power Sources 160 (2006) 915–924.
[15] Chang-jun Liu, Gheorghi P. Vissokov, Ben W.L. Jang, Catalysis Today 72 (2002) 173–184.
[16] J.C. Legrand, A.M. Diamy, G. Riahi, Z. Randriamanantenasoa, M. Polisset-Thfoin, J. Fraissard, Catalysis Today 89 (2004) 177–182.
[17] Seung-Soo Kim, Hwaung Lee, Byung-Ki Na, Hyung Keun Song, Catalysis Today 89 (2004) 193–200.
[18] Chang-jun Liu, Kailu Yu, Yue-ping Zhang, Xinli Zhu, Fei He, Baldur Eliasson, Applied Catalysis B: Environmental 47 (2004) 95–100.
[19] Yue-Ping Zhang, Pei-Sheng Ma, Xinli Zhu, Chang-Jun Liu, Yutian Shen, Catalysis Communications 5 (2004) 35–39.
[20] Xinli Zhu, Pei-pei Huo, Yue-ping Zhang, Chang-jun Liu, Industrial & Engineering Chemistry Research 45 (25) (2006) 8604–8609.
[21] Xinli Zhu, Pei-pei Huo, Yue-ping Zhang, Chang-jun Liu, Industrial & Engineering Chemistry Research 45 (2006) 8604–8609.
[22] Zhou-jun Wang, Yu Zhao, Lan Cui, Haiyan Du, Pei Yao, Chang-jun Liu, Green Chemistry 9 (2007) 554–559.
[23] Ji-Jun Zou, Yue-ping Zhang, Chang-Jun Liu, Langmuir 22 (2006) 11388–11394.